Original article

Molecular dynamics simulations of oil recovery from dolomite slit nanopores enhanced by CO_2 and N_2 injection

Huiying Guo[1,2]*, Ziqiang Wang[1,2], Bei Wang[1,2], Yuankai Zhang[1,2], Haojin Meng[1,2], Hongguang Sui[3]*

[1]*Research Institute of Experiment and Detection, Xinjiang Oilfield Company, Karamay 834000, P. R. China*
[2]*Xinjiang Laboratory of Shale Oil Exploration and Development, Karamay 834000, P. R. China*
[3]*College of Science, China University of Petroleum, Qingdao 266580, P. R. China*

Abstract:
Shale oil reservoirs are dominated by micro- and nanopores, which greatly impede the oil recovery rates. CO_2 and N_2 injection have proven to be highly effective approaches to enhance oil recovery from low-permeability shale reservoirs, and also represent great potential for CO_2 sequestration. Therefore, a better understanding of the mechanism of shale oil recovery enhanced by CO_2 and N_2 is of great importance to achieve maximum shale oil productivity. In this paper, the adsorption behavior of shale oil and the mechanism of enhancing shale oil recovery by CO_2 and N_2 flooding in dolomite slit pores are investigated by performing nonequilibrium molecular dynamics simulations. Considering the shale oil adsorption behavior, mass density distribution is analyzed and the results indicate that a symmetric density distribution of the oil regarding the center in the slit pore along the *x*-axis can be obtained. The maximum density of the adsorbed layer nearest to the slit wall is 1.310 g/cm^3 for C_8H_{18}, which is about 2.0 times of that for bulk oil density in the middle area of slit pore. The interaction energy and radial distribution functions (between oil and CO_2, and between oil and N_2) are calculated to display the displacement behavior of CO_2 and N_2 flooding. It is found that CO_2 and N_2 play different roles: CO_2 has strong solubility, diffusivity and a higher interaction energy with dolomite wall, and the oil displacement efficiency of CO_2 reaches 100% after 1 ns of flooding; however, during N_2 flooding, the oil displacement efficiency is 87.3% after 4 ns of flooding due to the lower interaction energy between N_2 and dolomite and that between N_2 and oil.

1. Introduction

With the development of modern industrial technology, such as horizontal drilling and hydraulic fracturing, the exploitation of shale oil can influence the global energy supply and subsequently mitigate the worldwide energy crisis and environmental issues, which has led to a "shale revolution" (Hughes, 2013; Zeng et al., 2020; Cai et al., 2022). Many scholars have studied the properties of oil in shale by performing empirical calculations (Panja et al., 2019; Wu et al., 2019; Zhao et al., 2020) and macroscopic simulation experiments (Tovar et al., 2020). The adsorption behavior and transport mechanism were reported as highly complex

and difficult to understand due to the pervasive presence of nanopore throat networks and the extremely small permeability of the shale matrix (de Almeida and Miranda, 2016; Yang et al., 2020). Omnipresent nanopores and low permeability present significant challenges during oil exploitation processes for shale (Wu et al., 2020).

In recent years, both theoretical and experimental methods as well as some field tests (Seyyedsar and Sohrabi, 2017; Singh, 2018) were broadly applied for extracting crude oil by CO_2 injection. Han et al. (2016) studied the effects of gravity segregation on both oil production and CO_2 sequestration by a 2D CO_2 flooding apparatus in vertical and horizontal
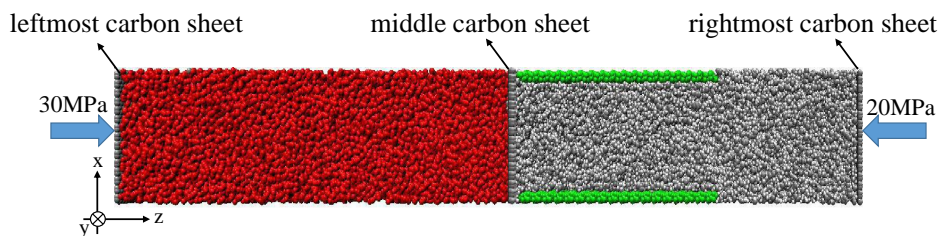
Fig. 1. Snapshot of the initial system configurations (red, CO_2 molecules; green, dolomite pore; gray, C_8H_{18} molecules).

sandstone systems, and the results indicated that the CO_2 has better storage efficiency in a miscible system. Zhou et al. (2019) conducted three types of CO_2 injection experiments to study oil production in a tight oil reservoir. The results revealed that the best method for enhanced oil recovery (EOR) was the injection of CO_2 in tight formations, and the crude oil recovery was indicated to reach 38.96%.

Despite the above advancements, some obvious disadvantages of CO_2 enhanced oil recovery have emerged, for example, higher production costs. Compared with CO_2, N_2 has the advantages of low cost, no corrosion, sufficient supply and ease of maintaining formation pressure (Potoff and Siepmann, 2001). It is widely known that the minimum miscibility pressure of gas-oil is a key parameter to evaluate the cost and feasibility of miscible flooding of gas EOR. Miscible N_2 flooding is a relatively rarely applied EOR technology in most oil reservoirs due to the requirement of high pressure to reach miscibility (Mogensen and Xu, 2020), which may lead to unexpectedly low replacement efficiency (Siregar et al., 2007). Mogensen and Xu (2020) found that miscible N_2 injection was a viable option to increase oil recovery. The density and viscosity of reservoir fluid could be increased by N_2 injection and the oil recovery was 10%-20% higher than that for water flood.

A direct and convenient approach to study the properties of oil in shale is to perform experiments (Anovitz and Cole, 2015; Gu et al., 2015; Haagh et al., 2018); however, the effect of surface anisotropy and high-pressure conditions, like those of the formation pressure in shale, cannot be easily predicted in this way. Scanning electron microscopy can clearly visualize the nanopores (Curtis et al., 2010; Eberle et al., 2016), but the pore structure or surface of rock samples possibly get damaged in the process. Although lab studies can well demonstrate the oil displacement efficiency by the injection of CO_2 or N_2, they cannot be used to explain the complex interactions, such as the changes in viscosity, density, specific volume, and swelling of crude oil after CO_2 or N_2 injection, or the oil displacement mechanism at the molecular level.

In the past few years, molecular dynamics by simulation has proved as a useful tool for studying the dynamical, structural properties in microscopic scale, and reveal the spatial distribution and trajectory of gas and oil molecules (Sui and Yao, 2016; Mohammed and Gadikota, 2019; Aminian and ZareNezhad, 2021). Mejía et al. (2014) combined experiments and molecular simulations to investigate the mixing processes of CO_2-oil molecules on tension measurements, coexisting densities, density profiles, and relative Gibbs adsorption

isotherms regarding the interfacial region. Fang et al. (2021) performed molecular simulations to study the behavior of gas injection and reveal the interaction between gas and oil at different reservoir depths. Zhang et al. (2021) found that CO_2 was preferably adsorbed on the calcite wall surface, forming a thin CO_2 film based on strong the interaction between oil and CO_2 molecules.

In this work, to address the issues mentioned above, the behaviors during the oil displacement process of CO_2 and N_2 injection and adsorption were studied by molecular simulations. First, the adsorption behavior was analyzed to reveal the oil distribution characteristics. Then, by scrutinizing the microscopic interaction, adsorption characteristics, and interface effect during the flooding process, the mechanism of migration behavior for shale oil was revealed. Dolomite, which has attracted many scholars' attention in subject areas (Tutolo et al., 2014; Berninger et al., 2017), was selected as reservoir matrix due to it being a common rock-forming mineral in carbonate reservoirs.

2. Methodology

2.1 Molecular models

Dolomite is the main component of shale in the Permian Lucaogou Formation of the Jimusar sag, which was selected as a typical mineral component. A repeat unit of dolomite was cleaved along the crystallographic orientation (1 -1 0) (Sui et al., 2020), and then a dolomite model supercell was rebuilt with dimensions of $x = 65.45$ Å, $y = 38.51$ Å and $z = 138.83$ Å to meet the slit pore width of 57 Å.

Saturated linear alkanes-octane (C_8H_{18}) was used to represent shale oil in the present work (Wang et al., 2015). The oil molecules were placed in the dolomite pore. All oil molecules were considered fully flexible, and a 4 ns equilibrium molecular dynamics simulation with a timestep of 1 fs on the simulation box with the canonical ensemble was performed to reduce the energy state and obtain a reasonable oil density. The gas (CO_2 or N_2) box was positioned on the left side of the dolomite slit pore to generate a pressure differential along the z-axis. The simulation model is shown in Fig. 1.

2.2 Simulation methods

The Large-scale Atomic/Molecular Massively Parallel Simulator package (Plimpton, 1995) was used to perform all of the molecular dynamics simulations. The interactions between atoms were described by the COMPASS (condensed-phase optimized molecular potential for atomistic simulation studies)

class II force field (Sun, 1998; Sun et al., 2016). This force field is expressed by:

$$E = E_{val} + E_{cro} + E_{non} \tag{1}$$

$$
\begin{aligned}
E_{val} = &\sum_b [A_2(b-b_0)^2 + A_3(b-b_0)^3 + A_4(b-b_0)^4] \\
&+ \sum_\phi [B_2(\phi-\phi_0)^2 + B_3(\phi-\phi_0)^3 + B_4(\phi-\phi_0)^4] \\
&+ \sum_\gamma [C_1(1-\cos\gamma) + C_2(1-\cos2\gamma) + C_3(1-\cos3\gamma)] \\
&+ \sum_\chi D\chi^2
\end{aligned} \tag{2}
$$

$$
\begin{aligned}
E_{cro} = &\sum_{b,b'} H_{bb}(b-b_0)(b-b_0') + \sum_{b,\phi} H_{b\phi}(b-b_0)(\phi-\phi_0) \\
&+ \sum_{b,\gamma} (b-b_0)(H_1\cos\gamma + H_2\cos2\gamma + H_3\cos3\gamma) \\
&+ \sum_{\phi,\gamma} (\phi-\phi_0)(F_1\cos\gamma + F_2\cos2\gamma + F_3\cos3\gamma) \\
&+ \sum_{b,\phi} V(\phi-\phi_0)(\phi-\phi_0') + \sum_{b,\phi,\gamma} Y(\phi-\phi_0)(\phi-\phi_0')
\end{aligned} \tag{3}
$$

$$
\begin{aligned}
E_{non} = &E_{vdW} + E_{ele} \\
= &\sum \varepsilon_{LJ} \left[2\left(\frac{r_{ij}^0}{r_{ij}}\right)^9 - 3\left(\frac{r_{ij}^0}{r_{ij}}\right)^6 \right] + \sum \frac{q_i q_j}{r_{ij}}
\end{aligned} \tag{4}
$$

The E_{val}, E_{cro}, E_{non}, E_{vdW} and E_{ele} represent valence energy, cross-term interaction energy, non-bonding interaction term, van der Waals interaction energy and electrostatic interaction energy, respectively. In Eqs. (1)-(4), q_i and q_j denote the charge of the i-th and j-th atoms, ε_{LJ} denotes the dielectric constant, and r_{ij} is the distance between atom i and atom j atomic. The parameters b, ϕ, γ and χ are bond length, bond angle, dihedral torsion angle and out of plane angle. b_0, b_0', ϕ_0, ϕ_0', A_i ($i = 1-4$), B_i ($i = 2-4$), C_i ($i = 1-3$), D, H_{bb}, $H_{b\phi}$, H_i ($i = 1-3$), F_i ($i = 1-3$), V and Y are fitted by quantum mechanical calculations. The parameters for dolomite, CO_2 and C_8H_{18} are listed in Table 1.

For this simulation step, firstly, the oil molecules were placed on the right side of the pore, and a carbon sheet (middle) was put on the left side of the dolomite pore to make it rigid and fixed. The fixed carbon sheet also kept oil away from CO_2 molecules before the flooding simulation, and 20 MPa pressure was applied to the rightmost carbon sheet along the z-axis to push the oil molecules into the pores. During the flooding simulation, the middle carbon sheet was removed, and 30 MPa pressure was applied to the leftmost carbon sheet along the z-axis to ensure the pressure difference of 10 MPa between the two sheets. Then, the CO_2 molecules were pushed into the pores to drive the oil phase across the channel.

All molecular dynamics simulations were performed by a canonical ensemble using the Velocity Verlet algorithm (Yoshida, 1990). The integration step was set as 1.0 fs, and 15.0 ns of simulation was conducted. Next, the trajectories were collected and used for data analysis, followed by the discussion of the properties of oil or gas in dolomite slit nanopores. The Nose–Hoover method (Martyna et al., 1994) was employed to control the temperature of the system, which was kept at 333 K. The van der Waals (vdW) interactions were calculated within a cutoff distance of 10.5 Å, and the particle-particle-particle-mesh (pppm) summation method (Hockney et al., 1974) with a relative error of 1×10^{-5} used to calculate the long-range interactions. Periodic boundary conditions were applied in all three dimensions. The configuration snapshots were rendered by visual molecular dynamics software (Fernandes et al., 2019).

3. Results and discussion

3.1 Density distribution

Prior to gas injection development, the mass density profiles of oil phase in the dolomite slit pores were calculated. The oil phase density could be computed based on the molecular centroid. Here, the slit pores were first divided into some slabs along the x direction, with each slab at 0.5 Å, and then the mass density could be determined in each slab (Wang et al., 2021). Fig. 2 shows the alkane density distributions in the dolomite slit pore. Obviously, a symmetric density distribution of C_8H_{18} regarding the pore center can be obtained. The oscillations of density distribution indicate that oil molecules form 4 similar layered adsorption structures near the two opposing walls. The result shows that oil molecules are subjected to large forces from the wall confined in nanoscale mineral pores, such as vdW and electrostatic interactions. Due to the high energy barrier between the adsorption layers, the dense adsorbed layer will limit the movement of oil molecules. The width of each adsorption layer between two adjacent density peaks (or valleys) was 5.0 Å, which is consistent with the measurement of solvation force (Christenson et al., 1987), and similar to those from previous studies (Wang et al., 2016; Sui et al., 2020). The first adsorption layer mass density was 1.322 g/cm^3 for C_8H_{18}, which is about 2.0 times greater than that for bulk oil phase density in the pore center. In the pore center, the density of C_8H_{18} was 0.661 g/cm^3, in good agreement with the result (0.659 g/cm^3) predicted by the National Institute of Standards and Technology Chemistry WebBook, which enhanced the correctness of our simulation and validates the simulation method.

Table 1. LJ-9-6 function parameters for dolomite, CO_2 and C_8H_{18}.

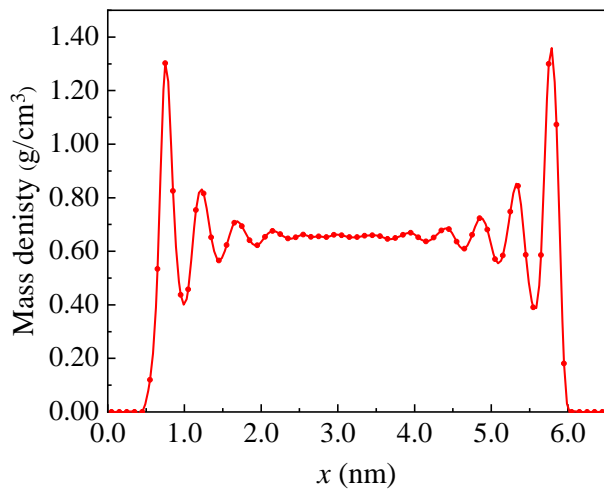|	ε (kcal/mol)	r^0 (Å)
O (dolomite)	0.067	3.360
Ca (dolomite)	0.112	3.400
Mg (dolomite)	0.046	2.600
C (dolomite)	0.070	3.900
C (CO_2)	0.068	3.915
O (CO_2)	0.067	3.360
C (C_8H_{18})	0.062	3.854
H (C_8H_{18})	0.023	2.878

Fig. 2. Mass density for C_8H_{18} in dolomite slit pore before gas flooding (20 MPa, 333 K).

3.2 Displacement behavior of CO_2 and N_2

A number of snapshots of the CO_2 injection process, the density variation of C_8H_{18} and CO_2 along the z-axis, and the number of C_8H_{18} and CO_2 at different times in dolomite slit pores are shown in Fig. 3. At $t = 0$ ns, there is an obvious interface between oil and gas, and oil molecules stay and are absorbed on the dolomite surface. With the time passing, the CO_2 molecules are injected into the dolomite pore, and they will occupy the position of oil molecules and replace them. CO_2 will also replace oil molecules adsorbed on the wall and create a film between them and the wall, as seen in Fig. 3(d), which is important for the separation of oil molecules from the dolomite surface and is beneficial to oil recovery. After 0.5 ns of flooding, the density profiles along the z-axis within the slit pore were computed to present a detailed density profile of the CO_2 and oil mixtures in Fig. 3(b), which showed that the density difference at the flooding frontier was gradual, and
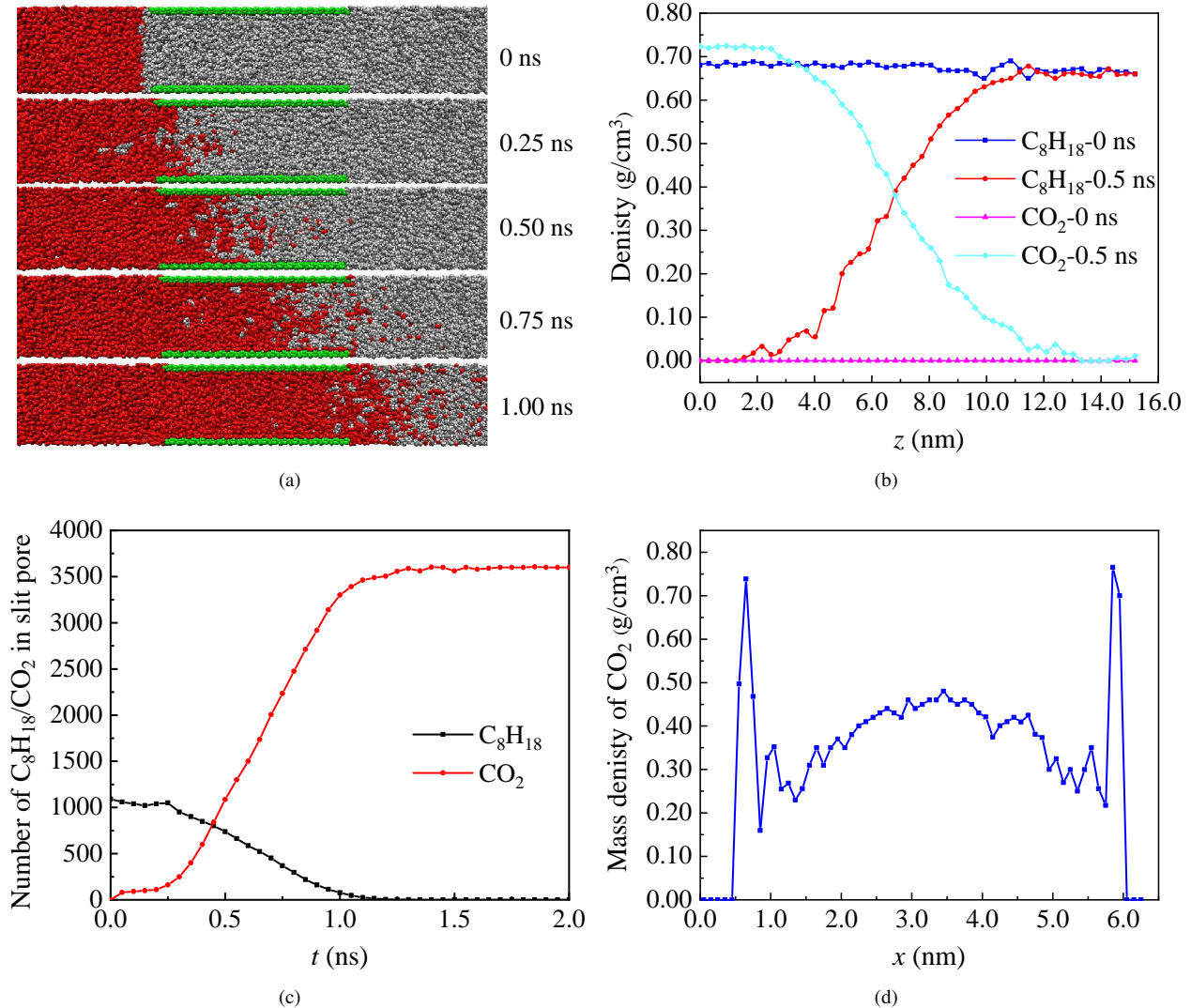

Fig. 3. (a) Snapshots to indicate the evolutions of CO_2 flooding (red: CO_2 molecule, gray: oil phase, green: dolomite); (b) Density profiles along the z-axis within the slit pore; (c) Amount of CO_2 and residual oil molecules in nanoslit during CO_2 flooding; (d) Density profiles of CO_2 along the x-axis within the slit pore after 0.5 ns of flooding.
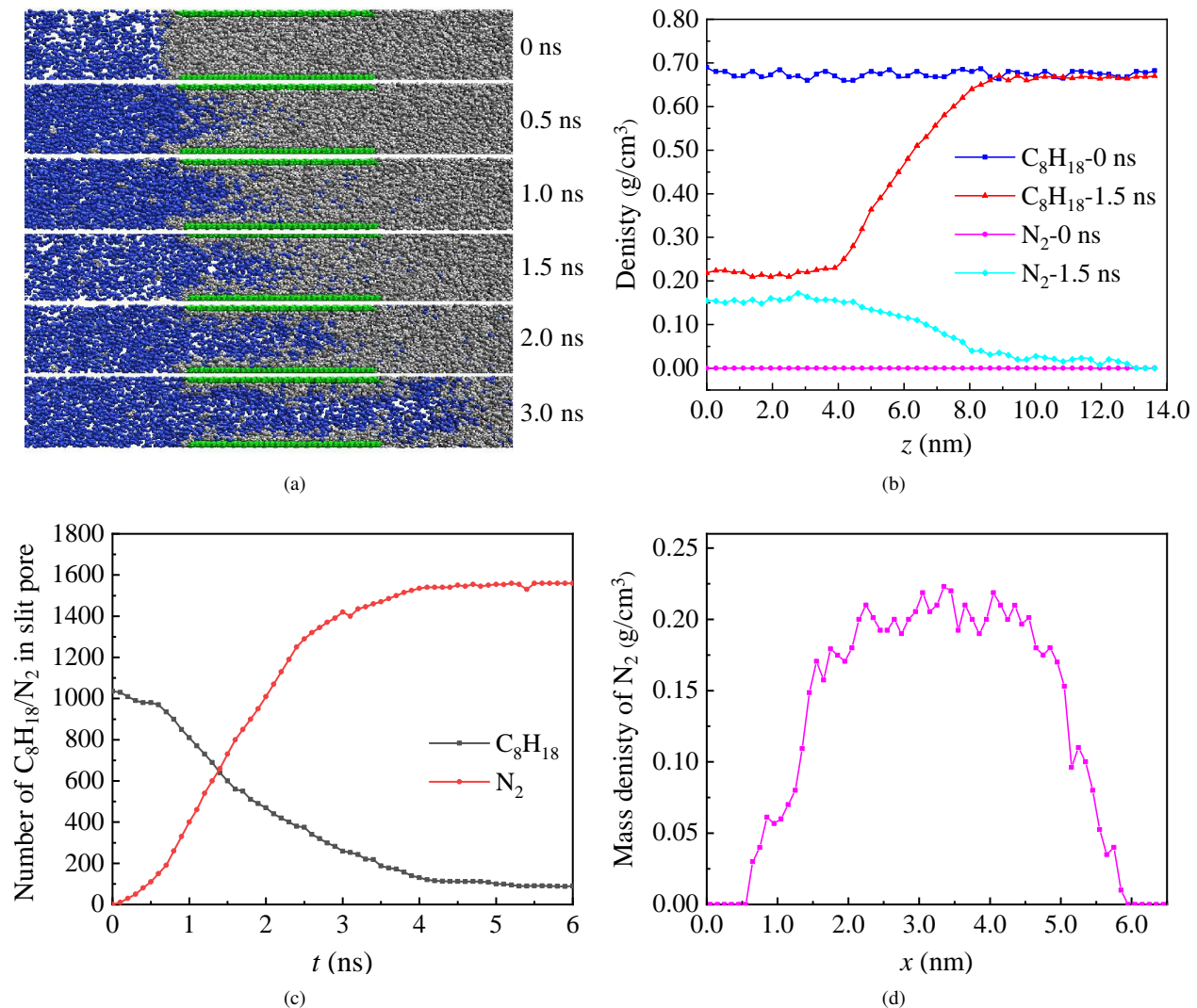
(a)

(b)

(c)

(d)

Fig. 4. (a) Snapshots depicting the evolutions of N_2 flooding (blue: N_2 molecule, gray: oil phase, green: dolomite); (b) Density profiles along the z-axis within the slit pore; (c) Number of N_2 and residual oil molecules in nanoslits during N_2 flooding; (d) Density profiles of N_2 along the x-axis within the slit pore after 2.0 ns of flooding.

there was actually no obvious interface between CO_2 and oil. In other words, almost all CO_2 molecules were dissolved in the oil phase at the gas-oil interface, indicating the good solution and diffusion properties of CO_2 molecules. Fig. 3(c) shows the amount of CO_2 and oil molecules in slit pores after CO_2 flooding. It is seen that after 1.0 ns of CO_2 flooding, almost all oil molecules have been driven out of the slit pores.

Fig. 4. shows the N_2 injection snapshots, the density of C_8H_{18} and N_2 along the z-axis, and the number of C_8H_{18} and N_2 at different time points in the dolomite slits. There is also an obvious interface between the oil and N_2 molecules; oil molecules remain and are absorbed on the dolomite surface at 0 ns. The snapshots in Fig. 4(a) indicate that there is an interface between N_2 and oil from the flooding frontier at different time points. Fig. 4(b) shows the density curve of oil and N_2 along the z-axis after 1.5 ns of flooding. From the figure, we can find that the density variation interval from 4 to 8 nm within the dolomite slit pore is shorter than that

during CO_2 flooding (after 0.5 ns of flooding, from 2 to 10 nm, see Fig. 3(b)), which means that the N_2 molecules have poor dissolution and diffusion properties compared to CO_2 in C_8H_{18} molecules. Fig. 4(c) depicts the number of oil and N_2 molecules remaining in the slit pores of N_2 flooding. It can be found that some oil molecules remain near the pore walls after 4 ns of N_2 flooding. Fig. 4(d) illustrates the density profiles of N_2 along the x-axis within the slit pore after 2.0 ns of flooding. Clearly, the N_2 density is low near the wall surface, indicating that oil molecules at the wall have not been displaced, that is, as for the N_2 injection, the N_2 molecules form a dominant path and pass through the oil phase in the slit pores.

The variation of oil molecule number during CO_2 and N_2 flooding within dolomite slit pores was studied and presented above in Figs. 3 and 4. These results show that the CO_2 molecules have better dissolution and diffusion properties than the N_2 molecules. During CO_2 flooding, almost all oil molecules will be driven out, but there will be some oil
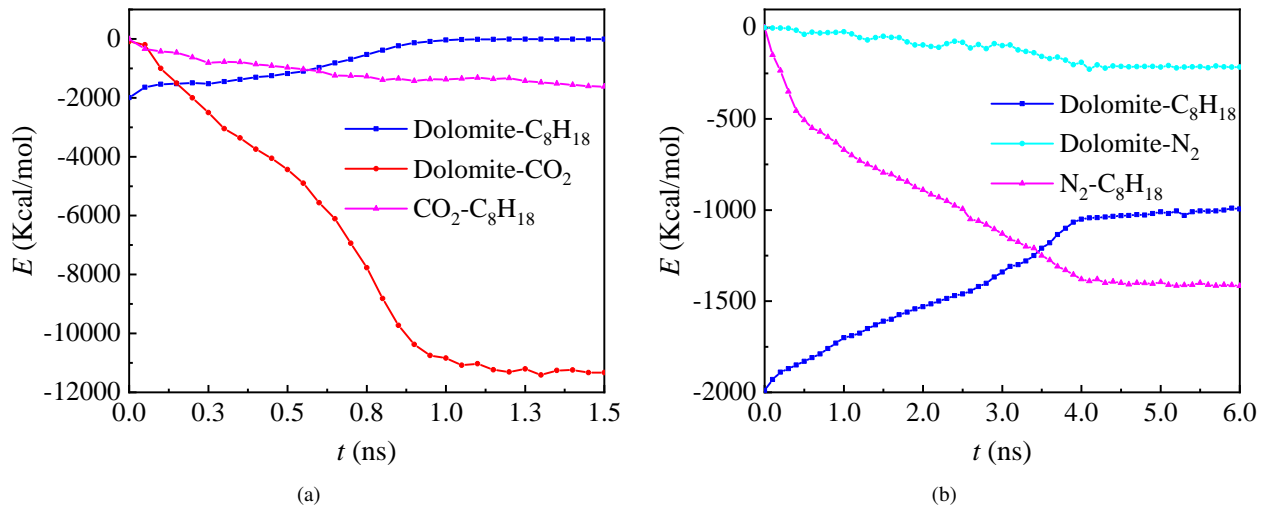
Fig. 5. Interaction energy profiles between oil molecules and dolomite wall under (a) CO_2 injection, and (b) N_2 injection.

molecules staying within the slit pores after the N_2 injections.

In order to clarify the nature of flooding behaviour, i.e., the dissolution and retention of octane during CO_2 and N_2 flooding, the interactions between gas phase, dolomite wall and the oil molecules were studied as shown in Fig. 5. The interaction energy can be computed by Eq. (5) (Li et al., 2016). Here, the interaction energy between octane and gas is displayed as follows:

$$E_{int} = E_{total} - (E_{gas} - E_{oct}) \qquad (5)$$

where E_{int} represents the interaction energy between gas and octane, E_{total} represents the total energy, and E_{gas} and E_{oct} denote the gas and the octane energy, respectively.

Fig. 5(a) shows the interaction energy of dolomite-CO_2, dolomite-C_8H_{18} and C_8H_{18}-CO_2 during CO_2 flooding. We can find that the interaction energy between dolomite wall and CO_2 increases gradually with time until 1 ns of CO_2 flooding. On the contrary, the interaction energy between dolomite wall and C_8H_{18} decreases gradually with time up to 1 ns when CO_2 molecules have filled the pores and all oil molecules have been driven out. The interaction energy between dolomite wall and CO_2 is greater than that between the dolomite wall and C_8H_{18} molecules, hence CO_2 can occupy the dolomite surface and expel oil molecules from the dolomite surface. In addition, the high attraction between C_8H_{18} and CO_2 can cause the CO_2 molecules to disperse into the C_8H_{18} phase, which can enhance the C_8H_{18} mobility due to its reduced viscosity.

Fig. 5(b) demonstrates the interaction energy of dolomite-N_2, dolomite-C_8H_{18} and C_8H_{18}-N_2. During N_2 flooding, the interaction energy between dolomite and N_2 is always smaller than that between dolomite and C_8H_{18} molecules during the whole flooding process from 0 to 6 ns. Thus, the N_2 molecules cannot peel off the oil molecules adsorbed on the dolomite surface.

Radial distribution function (RDF) can describe the probability of finding gas molecules at distance r from the oil molecule, which was calculated by:
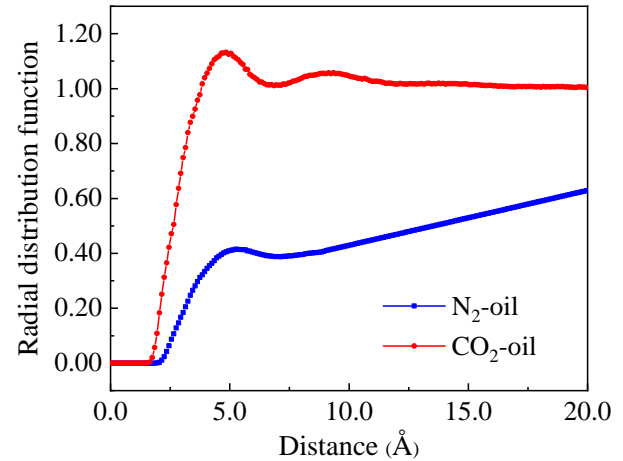

Fig. 6. Radial distribution function for the molecular mass centers of CO_2-C_8H_{18} and N_2-C_8H_{18}.

$$g(r) = \frac{\rho(r)}{\rho_0} \qquad (6)$$

where $\rho(r)$ represents the local density and ρ_0 is the bulk density.

Fig. 6 shows the RDFs between the CO_2 or N_2 and oil molecules after 0.5 ns of CO_2 flooding and 1.5 ns of N_2 flooding. It can be found that the first peak of RDF between CO_2 and oil molecules is located at 4.8 Å (line red), whereas the first peak of RDF between N_2 and oil molecules is lower at 5.3 Å (line blue). Hence, the interaction between CO_2 and oil molecules is stronger than that for N_2, which once again proves that CO_2 dissolves more easily in the oil phase.

Overall, the homogeneous conceptual slit model of dolomite on oil recovery was simulated at the nanoscale, which revealed the oil distribution and displacement process by density. We believe that these findings improve the understanding of CO_2-EOR and N_2-EOR process and benefit practical oil exploitation activities. However, our conceptual model of homogenization has limitations, it does not consider pore shape, roughness and matrix type, and the models are too

small, causing the simulation results to deviate from the real results. Further studies should be conducted at the macroscale simulations, whose scale is closer to the practical scale of underground oil reservoirs.

4. Conclusions

In the present study, the recovery of oil molecules from dolomite slit pore by CO_2 and N_2 flooding was investigated using molecular dynamics simulations, and the results showed that CO_2 and N_2 play different roles in the flooding process. CO_2 molecules have good dissolution and diffusion properties for replacing oil. The interaction energy between dolomite and CO_2 is stronger than that between dolomite and C_8H_{18}, thereby CO_2 can easily dislodge the oil adsorbed on the dolomite surface. For our dolomite slit pore model, at a pressure differential of 10 MPa and temperature of 333 K, CO_2 can dissolve and completely displace oil molecules, and the oil displacement efficiency can reach 100% after 1 ns of flooding. On the other hand, N_2 molecules cannot completely displace oil molecules adsorbed on dolomite surface due to the lower interaction energy between dolomite and N_2, and the oil displacement efficiency is 87.3% after 4 ns of flooding.

Acknowledgement

Conflict of interest

The authors declare no competing interest.

References

Aminian, A., ZareNezhad, B. Molecular dynamics simulations study on the shear viscosity, density, and equilibrium interfacial tensions of CO_2 + brines and brines + CO_2 + n-decane systems. The Journal of Physical Chemistry B, 2021, 125(10): 2707-2718.

Anovitz, L. M., Cole, D. R. Characterization and analysis of porosity and pore structures. Reviews in Mineralogy and Geochemistry, 2015, 80(1): 61-164.

Berninger, U., Saldi, G. D., Jordan, G., et al. Assessing dolomite surface reactivity at temperatures from 40 to 120 °C by hydrothermal atomic force microscopy. Geochimica et Cosmochimica Acta, 2017, 199: 130-142.

Cai, J., Wood, D. A., Hajibeygi, H., et al. Multiscale and multiphysics influences on fluids in unconventional reservoirs: Modeling and simulation. Advances in Geo-Energy Research, 2022, 6(2): 91-94.

Christenson, H. K., Gruen, D. W. R., Horn, R. G., et al. Structuring in liquid alkanes between solid surfaces: Force measurements and meanfield theory. The Journal of Chemical Physics, 1987, 87(3): 1834-1841.

Curtis, M. E., Ambrose, R. J., Sondergeld, C. H. Structural characterization of gas shales on the micro- and nano-scales, Paper SPE 137693 Presented at Canadian Unconventional Resources and International Petroleum Conference, Calgary, Alberta, Canada, 19-21 October, 2010.

de Almeida, J. M., Miranda, C. R. Improved oil recovery in nanopores: NanoIOR. Scientific Reports, 2016, 6: 28128.

Eberle, A. P. R., King, H. E., Ravikovitch, P. I., et al. Direct measure of the dense methane phase in gas shale organic porosity by neutron scattering. Energy & Fuels, 2016, 30(11): 9022-9027.

Fang, T., Li, S., Zhang, Y., et al. How the oil recovery in deep oil reservoirs is affected by injected gas types: A molecular dynamics simulation study. Chemical Engineering Science, 2021, 231: 116286.

Fang, T., Wang, M., Li, J., et al. Study on the asphaltene precipitation in CO_2 flooding: A perspective from molecular dynamics simulation. Industrial & Engineering Chemistry Research, 2018, 57(3): 1071-1077.

Fernandes, H. S., Sousa, S. F., Cerqueira, N., VMD store-a VMD plugin to browse, discover, and install VMD extensions. Journal of Chemical Information and Modeling, 2019, 59(11): 4519-4523.

Gu, X., Cole, D. R., Rother, G., et al. Pores in marcellus shale: A neutron scattering and FIB-SEM study. Energy & Fuels, 2015, 29(3): 1295-1308.

Haagh, M. E. J., Schilderink, N., Duits, M. H. G., et al. Salinity-dependent contact angle alteration in oil/brine/silicate systems: The effect of temperature. Journal of Petroleum Science and Engineering, 2018, 165: 1040-1048.

Han, J., Lee, M., Lee, W., et al. Effect of gravity segregation on CO_2 sequestration and oil production during CO_2 flooding. Applied Energy, 2016, 161: 85-91.

Hockney, R., Goel, S., Eastwood, J. Quiet high-resolution computer models of a plasma. Journal of Computational Physics, 1974, 14(2): 148-158.

Hughes, J. D. Energy: A reality check on the shale revolution. Nature, 2013, 494(7437): 307-308.

Li, X., Xue, Q., Zhu, L., et al. How to select an optimal surfactant molecule to speed up the oil-detachment from solid surface: A computational simulation. Chemical Engineering Science, 2016, 147: 47-53.

Martyna, G. J., Tobias, D. J., Klein, M. L. Constant pressure molecular dynamics algorithms. The Journal of Chemical Physics, 1994, 101(5): 4177-4189.

Mejía, A., Cartes, M., Segura, H., et al. Use of equations of state and coarse grained simulations to complement experiments: Describing the interfacial properties of carbon dioxide + decane and carbon dioxide + eicosane mixtures. Journal of Chemical & Engineering Data, 2014, 59(10): 2928-2941.

Mogensen, K., Xu, S. Comparison of three miscible injectants for a high-temperature, volatile oil reservoir - With particular emphasis on nitrogen injection. Journal of Petroleum Science and Engineering, 2020, 195: 107616.

Mohammed, S., Gadikota, G., CO_2-Induced displacement and

diffusive transport of shale geofluids in silica nanopores of varying sizes. Journal of CO_2 Utilization, 2019, 32: 37-45.

Panja, P., Pathak, M., Deo, M. Productions of volatile oil and gas-condensate from liquid rich shales. Advances in Geo-Energy Research, 2019, 3(1): 29-42.

Plimpton, S. Fast parallel algorithms for short-range molecular dynamics. Journal of Computational Physics, 1995, 117(1): 1-19.

Potoff, J. J., Siepmann, J. I. Vapor–liquid equilibria of mixtures containing alkanes, carbon dioxide, and nitrogen. AIChE Journal, 2001, 47(7): 1676-1682.

Seyyedsar, S. M., Sohrabi, M. Intermittent CO_2 and viscosity-reducing gas (VRG) injection for enhanced heavy oil recovery. Fuel Processing Technology, 2017, 164: 1-12.

Singh, H. Impact of four different CO_2 injection schemes on extent of reservoir pressure and saturation. Advances in Geo-Energy Research, 2018, 2(3): 305-318.

Siregar, S., Hidayaturobbi, A., Wijaya, B., et al. Laboratory experiments on enhanced oil recovery with nitrogen injection. Journal of Engineering and Technological Sciences, 2007, 39(1): 20-27.

Sui, H., Yao, J. Effect of surface chemistry for CH_4/CO_2 adsorption in kerogen: A molecular simulation study. Journal of Natural Gas Science and Engineering, 2016, 31: 738-746.

Sui, H., Zhang, F., Wang, Z., et al. Molecular simulations of oil adsorption and transport behavior in inorganic shale. Journal of Molecular Liquids, 2020, 305: 112745.

Sun, H. COMPASS: An ab initio force-field optimized for condensed-phase applications overview with details on alkane and benzene compounds. The Journal of Physical Chemistry B, 1998, 102(38): 7338-7364.

Sun, H., Jin, Z., Yang, C., et al. COMPASS II: Extended coverage for polymer and drug-like molecule databases. Journal of Molecular Modeling, 2016, 22(2): 47.

Tovar, F. D., Barrufet, M. A., Schechter, D. S. Enhanced oil recovery in the wolfcamp shale by carbon dioxide or nitrogen injection: An experimental investigation. SPE Journal, 2020, 26(1): 515-537.

Tutolo, B. M., Luhmann, A. J., Kong, X. Z., et al. Experimental observation of permeability changes in dolomite at CO_2 sequestration conditions. Environmental Science & Technology, 2014, 48(4): 2445-2452.

Wang, S., Feng, Q., Javadpour, F., et al. Oil adsorption in shale nanopores and its effect on recoverable oil-in-place. International Journal of Coal Geology, 2015, 147–148: 9-24.

Wang, S., Javadpour, F., Feng, Q. Molecular dynamics simulations of oil transport through inorganic nanopores in shale. Fuel, 2016, 171: 74-86.

Wang, Y. X., Kiziltas, A., Blanchard, P., et al. Calculation of 1D and 2D densities in VMD: A flexible and easy-to-use code. Computer Physics Communications, 2021, 266: 108032.

Wu, K., Chen, Z., Li, J., et al. Nanoconfinement effect on n-alkane flow. The Journal of Physical Chemistry C, 2019, 123(26): 16456-16461.

Wu, T., Zhao, J., Zhang, W., et al. Nanopore structure and nanomechanical properties of organic-rich terrestrial shale: An insight into technical issues for hydrocarbon production. Nano Energy, 2020, 69: 104426.

Yang, Y., Liu, J., Yao, J., et al. Adsorption behaviors of shale oil in kerogen slit by molecular simulation. Chemical Engineering Journal, 2020, 387: 124054.

Yoshida, H. Construction of higher order symplectic integrators. Physics Letters A, 1990, 150(5-7): 262-268.

Zeng, Q., Yao, J., Shao, J. An extended finite element solution for hydraulic fracturing with thermo-hydro-elastic–plastic coupling. Computer Methods in Applied Mechanics and Engineering, 2020, 364: 112967.

Zhang, W., Feng, Q., Wang, S., et al. CO_2-regulated octane flow in calcite nanopores from molecular perspectives. Fuel, 2021, 286: 119299.

Zhao, G., Yao, Y., Adenutsi, C. D., et al. Transport behavior of oil in mixed wettability shale nanopores. ACS Omega, 2020, 5(49): 31831-31844.

Zhou, X., Yuan, Q., Zhang, Y., et al. Performance evaluation of CO_2 flooding process in tight oil reservoir via experimental and numerical simulation studies. Fuel, 2019, 236: 730-746.